

OSCILLATIONS AND HEATING OF THE SOLAR CORONA

C. A. Mendoza-Briceño,¹ A. Parravano,¹ and M. H. Ibáñez S.¹

RESUMEN

En este trabajo discutiremos las observaciones, consecuencias y modelamiento de las oscilaciones en lazos coronales, su amortiguamiento y su papel para proveer diagnósticos del plasma coronal, así como su relación con el problema fundamental del calentamiento de la corona.

ABSTRACT

In this paper we will discuss the observations, consequence and modelling of coronal loops oscillations. These oscillations and their damping are of fundamental importance, because they can provide diagnostics of the coronal plasma as well as insight of their role on the fundamental problem of the coronal heating.

Key Words: MHD — Sun: corona — Sun: oscillations

1. INTRODUCTION

Recent observations by high-resolution space imaging telescopes and spectrometers on board the *SOHO* and *TRACE* spacecrafts have delivered data of unprecedented quality that support the view of significant magnetohydrodynamic (MHD) wave activity in the solar corona. In response to this, coronal loop oscillations have become a subject of increasing theoretical interest. In particular, MHD waves, fast or slow, are natural carriers of energy and so they are likely sources for heating of the coronal plasma and for solar wind acceleration. They are also potentially valuable sources of seismic information, providing a coronal seismology (Roberts, Edwin, & Benz 1984; Nakariakov & Ofman 2001). There are three basic branches of solutions of the dispersion relation for propagating and standing MHD waves: the slow-mode branch (with acoustic phase speeds), the fast-mode branch and the Alfvén branch (with Alfvénic phase speeds). Furthermore, each branch has a symmetric and asymmetric solution, termed the sausage and kink modes (Roberts, Edwin, & Benz 1984). All of these MHD oscillation modes have been detected with imaging observations in recent years: transverse fast kink-mode oscillations with TRACE (Aschwanden et al. 1999; Nakariakov et al. 1999), longitudinal (slow magnetoacoustic) modes with SUMER (Wang et al. 2002a,b; Ofman & Wang 2002), and fast sausage mode oscillations, probably with the Nobeyama radioheliograph (Asai et al. 2001). The Solar Ultraviolet Measurements of Emitted Radiation (SUMER) spectrometer on board the SOHO satellite detected large Doppler

shift velocities with strong oscillatory damping in hot ($T > 6$ MK) coronal loops (Kliem et al. 2002; Wang et al. 2002a,b). These oscillations were interpreted as signatures of standing slow or kink magnetosonic waves excited impulsively in the loops (Ofman & Wang 2002). Moreover, Sakurai et al. (2002) presented a time sequence over 80 min of coronal green-line spectra obtained with a ground-based coronagraph at the Norikura Solar Observatory. They also detected Doppler shift oscillations and they have interpreted them as propagating, rather than standing, slow-mode MHD waves.

The relevance of observed MHD oscillations and propagating wave phenomena for coronal heating has been estimated (Aschwanden 2004), deriving first the energy fluxes that are contained in MHD waves and compare them with the radiative and conductive losses in the corona. Aschwanden (2004) found that MHD oscillations and waves with Alfvénic phase speeds have an energy flux that is comparable with coronal losses, while MHD oscillations and waves with acoustic phase speeds contain insufficient energy to balance coronal losses. Also dissipation of Alfvén waves can possibly account for coronal heating in coronal holes as well as in active regions, but their detection can only be facilitated by line broadening or by fast-mode MHD oscillations in resonant loops. Acoustic waves are easier to detect based on Doppler shifts and density modulation, but they seem to be irrelevant for coronal heating.

2. MODEL AND GOVERNING EQUATIONS

Since the plasma dynamics in a coronal loop is dominated by the magnetic field, a usual assumption is made, i.e. the plasma motion takes place primarily

¹Centro de Física Fundamental, Facultad de Ciencias, Universidad de los Andes, Mérida, Venezuela (cesar@ula.ve).

along the magnetic field lines, which in turn determines the loop geometry. The energy conservation reads as

$$\rho \frac{dT}{dt} = -\frac{\bar{\mu}(\gamma - 1)}{\mathcal{R}_g} \times \left[p \frac{\partial v}{\partial s} + \rho^2 Q(T) - H - \frac{\partial}{\partial s} \left(\kappa \frac{\partial T}{\partial s} \right) - \frac{4}{3} \eta \left(\frac{\partial v}{\partial s} \right)^2 \right], \quad (1)$$

where t is time, s denotes the position along a loop of constant cross-section, ρ is the plasma mass density, v is the fluid velocity, T is the plasma temperature, p is the gas pressure, $Q(T) = \chi T^\alpha$ is the optically thin radiation-loss function with χ and α the Hildner's (1974) cooling coefficient and exponent, respectively, H is the coronal heating function, $\gamma (= 5/3)$ is the ratio of specific heats, $\bar{\mu}$ is the mean molecular weight, $\kappa = 10^{-6} T^{5/2}$ ergs cm $^{-1}$ s $^{-1}$ K $^{-1}$ is the coefficient of thermal conductivity parallel to the magnetic field, and η is the coefficient of compressive viscosity (Braginskii 1965). Equation (1) together with the continuity and momentum equations are closed by assuming $p = \mathcal{R}_g \rho T / \bar{\mu}$, where \mathcal{R}_g is the gas constant.

3. RESULTS AND DISCUSSION

3.1. Oscillating coronal loops

The aim of this section is to quantify the effects of stratification on damping of the Doppler shift oscillations observed by SUMER in hot ($T > 6$ MK) coronal loops. To do so, we start from the same loop parameters used by Ofman & Wang (2002), who performed similar calculations of the damping of slow MHD waves in hot loops by neglecting the effects of solar gravity. In particular, we choose a one-dimensional loop configuration of semi-circular shape, constant cross-sectional area, and total length $L = 400$ Mm ($\approx 0.575 R_\odot$), with an initial uniform temperature ($T = 6.3$ or 8.0 MK) distribution. For the non-stratified models, an initial uniform density ($= 5.0 \times 10^8$ cm $^{-3}$) distribution is used. As outlined by Ofman & Wang (2002), these initial parameters are motivated by SUMER and Yohkoh/soft X-ray telescope (SXT) observations of hot loops in the upper solar atmosphere. With this choice, the coefficient of compressive viscosity takes values of $\eta \approx 9.58$ g cm $^{-1}$ s $^{-1}$ for $T = 6.3$ MK and ≈ 17.40 g cm $^{-1}$ s $^{-1}$ for $T = 8.0$ MK, while the coefficient of thermal conductivity is $\kappa \approx 9.96 \times 10^{10}$ ergs cm $^{-1}$ s $^{-1}$ K $^{-1}$ for $T = 6.3$ MK and $\approx 1.81 \times 10^{11}$ ergs cm $^{-1}$ s $^{-1}$ K $^{-1}$ for $T = 8.0$ MK.

Loop oscillations in the form of standing slow magnetosonic waves are introduced by allowing the

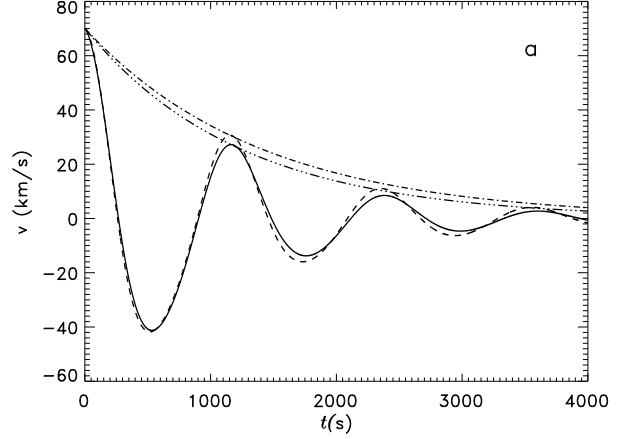


Fig. 1. Time evolution of the wave velocity at $s = l_0 = 0.35L$ for a loop model with $T = 8.0$ MK and $L = 400$ Mm. Waves in a stratified loop (solid line) are compared with those in a non-stratified medium (dashed line) for an initial wave-velocity amplitude of 84 km s $^{-1}$. The fits of the exponential wave damping are shown with the dot-dashed and triple-dot-dashed curves for the non-stratified and stratified loop, respectively.

initial velocity to oscillate with position along the loop with a prescribed constant amplitude v_0 . In order to check the ability of the code to reproduce the results obtained by Ofman & Wang (2002), we first consider initial wave-velocity amplitudes of 20 and 87 km s $^{-1}$ in a non-stratified loop model and then compare the results for the same parameters in the stratified case. Figures 1 and 2 display the resulting time evolution of the wave velocity and density at a fixed distance $l_0 = 0.35L (\approx 0.20 R_\odot)$ from the left footpoint at $s = 0$ for the case in which $T = 8.0$ MK and $v_0 = 87$ km s $^{-1}$. The solid line depicts the wave evolution in the stratified loop (i.e., with gravity included), while the dashed line shows the same evolution with no stratification (i.e., with no gravity). The fits of the exponential decay of the amplitude $v_0 \exp(-t/t_d)$, where t_d is the dissipation time, are also shown in Figure 1 with the dot-dashed (no stratification) and triple-dot-dashed (stratification) curves. In the stratified case, the wave velocity has a period of ≈ 1163 s (≈ 19.4 min) and a decay time of about 1231 s (≈ 20.5 min). For comparison, the wave in the non-stratified loop has a slightly shorter period (≈ 1153 s ≈ 19.2 min) and a longer decay time (≈ 1396 s ≈ 23.3 min). In both cases, the wave velocity almost completely dissipates after about 4000 s (≈ 66.7 min), with the wave in the stratified loop reaching smaller amplitudes ($v \approx 2.72$ km s $^{-1}$ by 3601 s) faster than in the non-stratified case ($v \approx 4.10$ km s $^{-1}$ by 3553 s).

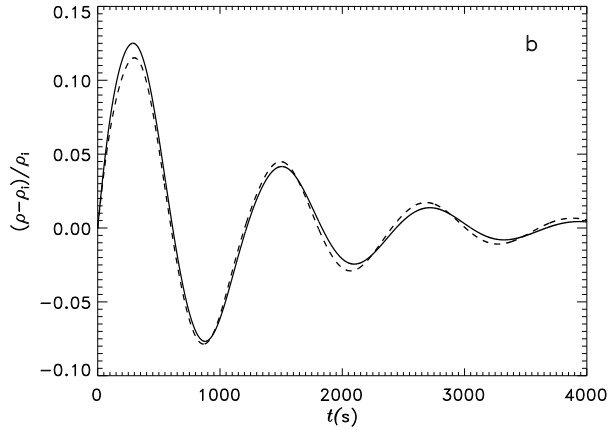


Fig. 2. Same as Fig. 1 but for the wave density.

The time evolution of the density perturbations calculated as $\delta\chi/\chi = [\chi(s = l_0, t) - \chi_i]/\chi_i$, where χ_i denotes the initial ($t = 0$) value of ρ at $s = l_0$, is shown in Figure 2.

We see that the density oscillation exhibits an $1/4$ -period phase difference compared to the velocity. This latter result supports the observational finding that for standing slow-mode waves in hot loops, the intensity fluctuations lag the Doppler shifts by a quarter period (Wang et al. 2003b). From Figure 1 we also see that the waves dissipate on essentially the same timescale independently of whether gravity is included or excluded. In the cooler ($T = 6.3$ MK) loops, the period and decay time of the slow waves are longer compared to those in the hotter ($T = 8.0$ MK) models.

In addition, the predicted ratio of decay time to period is ~ 1.6 for the $T = 6.3$ MK stratified and non-stratified loop models, whereas $t_d/P \sim 1.1$ and 1.2 for the stratified and non-stratified $T = 8.0$ MK models, respectively. These ratios are within the range of values (0.3–2.1) inferred observationally by Wang et al. (2003b) on the basis of data for 54 Doppler shift oscillations associated with 27 flux enhancement events of hot plasma.

The result that the decay time becomes shorter at higher temperatures is consistent with thermal conduction being the dominant mechanism for damping of coronal loop oscillations. In particular, in the stratified case when $T = 6.3$ MK the wave velocity has a period of ≈ 1306 s (≈ 21.8 min) and a decay time of ≈ 2062 s (≈ 34.4 min) for an initial wave amplitude of 87 km s^{-1} . These results compare favorably with the period (~ 16.8 min) and decay time (~ 36.8 min) measured by Wang et al. (2003a) for one Doppler shift oscillation produced by an M-class flare and recorded in an Fe XIX line by SUMER in

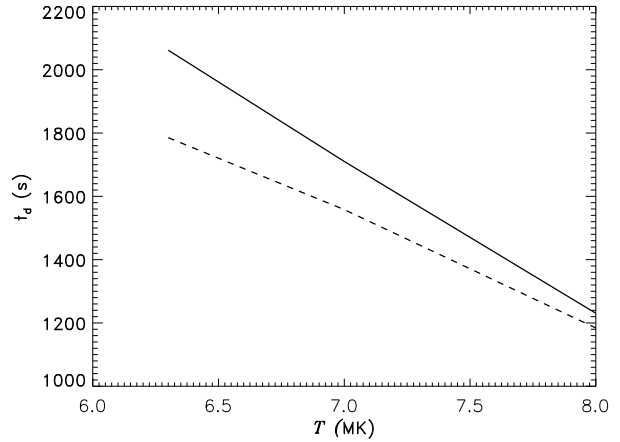


Fig. 3. Dependence of the decay time t_d on loop temperature T , as obtained from two independent sequences of calculations with fixed loop length (400 Mm) and varying temperatures from $T = 6.3$ to 8.0 MK. The solid and dashed lines correspond to $v_0 = 87$ and 20 km s^{-1} , respectively.

a loop with $T = 6.3$ MK and length $L = 191$ Mm. By about 4016 s the velocity at $s = l_0$ is ≈ 5.75 km s^{-1} , corresponding to approximately 8% of its value at $t = 0$. As expected, this amplitude is higher than the 4% value found for the hotter loop model at a comparable evolution time.

While the above predicted periods and decay times are toward the intermediate ($T = 8$ MK) and upper ($T = 6.3$ MK) parts of the range of values observed by *SOHO* in hot coronal loops, we find that the main effect of stratification is to reduce the dissipation time of slow-mode waves by $\sim 10 - 20\%$ compared to the non-stratified models.

We now study the variation of the decay time of standing slow-mode waves with temperature and total loop length in stratified hot loop models. In Figure 3 the damping time as a function of the temperature is shown for $v_0 = 20$ (dashed line) and 87 km s^{-1} (solid line), as obtained for two separate sequences of model calculations with fixed loop length (400 Mm) and varying temperatures from $T = 6.3$ to 8.0 MK.

We see that the decay time decreases linearly with temperature in stratified hot loops. It is evident that at any given temperature the decay time shortens for lower wave amplitudes. When $T = 6.3$ MK the damping time for $v_0 = 87$ km s^{-1} is about 300 s longer than when $v_0 = 20$ km s^{-1} . This difference reduces to about 60 s when the loop temperature is increased to $T = 8.0$ MK. Clearly, this occurs because the size of the wave amplitude affects the slope of the linear variation in the sense that the

higher is the value of v_0 , the faster is the decrease of the decay time with temperature. As a consequence, in hotter loops ($T \geq 8.0$ MK), slow MHD waves of differing amplitudes may have comparable decay times due to the increasing dissipative effects of thermal conduction at such high temperatures.

The dependence of the decay time on loop length was also studied for four separate sequences of model calculations with varying length from 100 to 400 Mm and fixed temperature and wave-velocity amplitude.

In general, as the loop length is increased, the decay time of slow magnetosonic waves also increases. The increase of the decay time with length is seen to occur at a much faster rate when $T = 6.3$ MK and $v_0 = 87$ km s⁻¹. When $T = 8.0$ MK, the decay time becomes essentially independent of the wave amplitude for the range of loop lengths considered. We also noted that for all sequences the increase of t_d with length was almost linear, which was expected because for standing slow magnetosonic waves $P \approx 2L/c_s$ (Roberts et al. 1984), where c_s is the sound speed. This approximate linear dependence of the period on loop length has also been found to match the observed periods rather well (Wang et al. 2003a,2003b). The fact that at higher temperatures the dissipation time of oscillations becomes shorter is again indicative of the overwhelming dissipative effects of thermal conduction in the hottest loops. Moreover, the evidence that for all sequences the shortest decay times occur in the smallest loops (of length 100 Mm) plays also in favor of thermal conduction as the primary mechanism for slow-mode wave dissipation.

3.2. Intermittent coronal loop oscillations

Mendoza-Briceño, Sigalotti, and Erdelyi (2005, hereafter MSE05), in their study of multiple spatio-temporal impulsive loop heating found that with a large number of pulses, having a fully random spatio-temporal distribution, the plasma stays at coronal temperatures during the impulsive heating stage. Variations in the randomness of the heat releases produced qualitatively similar evolutions, differing mainly in the spatio-temporal distribution of localized thermal bumps that appear randomly along the hottest loop segments. The model calculations also predicted the occurrence of sporadic and very rapid temperature depressions near the loop apex, which are always accompanied by equally rapid rises of the apex density. These depressions may involve strong temperature variations, most of them from $\sim 1.5 \times 10^6$ down to $\sim 10^4$ K, which may last from about 3 to 10 min, and their number may be sen-

sitive to the details of the spatio-temporal distribution of the microscale heating. MSE05 concluded that this behaviour may be related to the observed rapid time variability of coronal loops inferred from SoHO-CDS observations in active regions of the solar atmosphere (Kjeldseth-Moe & Brekke 1998; Schrijver 2001). Moreover, when the pulses are less concentrated near the loop's footpoints, the evolution produces hotter loops and progressively less flat temperature profiles in the upper parts of the loop along with an appreciably reduced number of the temperature depressions. This latter feature is consistent with the observational lack of strong variability at very high coronal temperatures (Kjeldseth-Moe & Brekke 1998; Schrijver 2001).

Here we discuss the oscillatory motions that are generated in the loop by random energy releases. For this purpose the time-distance density contour is presented in Figure 4. The panels of Figure 4 show the dynamic evolution of the plasma temperature, density and velocity (top, second and third panels of Figure 4) as well as the corresponding apex density and velocity (Figure 4 in the bottom panel).

3.3. Randomly driven global coherent oscillating pattern

Oscillatory motions are clearly visible as a series of light and dark bands (dark features indicate higher densities) on the density time-distance plot (second panel of Figure 4). Similar features can be seen on the velocity time-distance plot (third panel of Figure 4). On a movie-presentation of these data one can observe plenty of travelling acoustic waves during the entire evolution due to the random injections of pulses. Of course, the most interesting question is whether these random motions could manifest, even intermittently, in coherent dynamical signals of loop response that may be observable. One obvious candidate of such coherent apparent response would be the presence of standing waves. In what follows we investigate whether the coherent response in Figure 4 could be standing waves. In order to establish the nature of these oscillations one can analyse the variations of the relation between density and velocity at various locations of the loop. Inspecting Figure 4 (second and third panels) one can identify *in-phase* (or close to it) responses as *coherent* dark or light bands (second panel of Figure 4), e.g. between $t=600-1200$ s. Although the density response is intermittent, it seems to be in phase along the entire loop, while the corresponding velocity does not show a clear indication of the standing wave behaviour. It can be shown theoretically, that, for standing waves

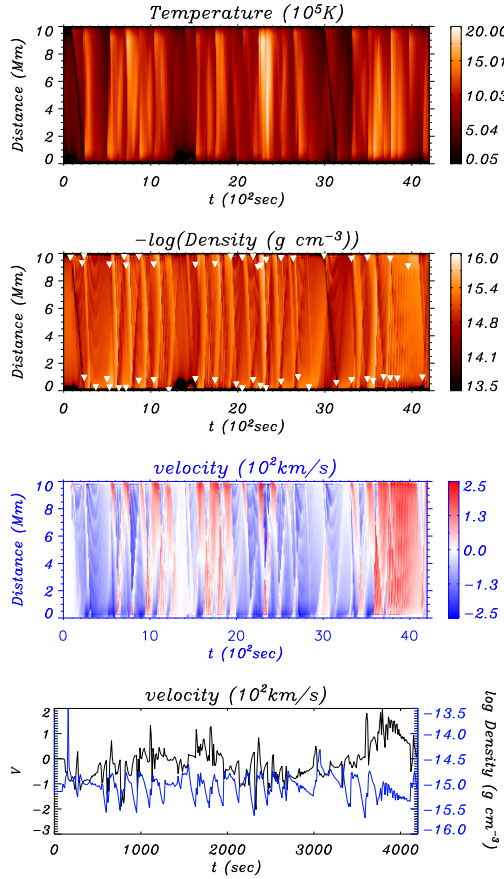


Fig. 4. Dynamical evolution of the temperature (upper panel), density (second panel) and velocity (third panel) along the loop as a function of coordinate s . The lower panel corresponds to the apex density and velocity as a function of time.

in a finite length, uniform magnetic flux tube there has to be a quarter phase shift between the velocity and density. The considered loop is stratified and non-isothermal. However, it can still be approximated by a uniform loop and one should expect, for standing waves, a quarter period phase shift (or close to it!) between density and velocity. The bottom panel of Figure 4 shows the time series of velocity and density at the apex point of the loop. The apex point is arbitrarily chosen, without any loss of generality. The velocity and density time series clearly show a phase shift of the order of $P/4$, where P is the period involved. The actual period will be established from the wavelet analysis of the density time series (see the top panel of Figure 5). One important feature in the panel of Figure 5 is the sporadic appearance of density rises that also correspond to temperature drops. Note, that the phase shift in Figure 4 (bottom panel) is sometimes close to a quarter

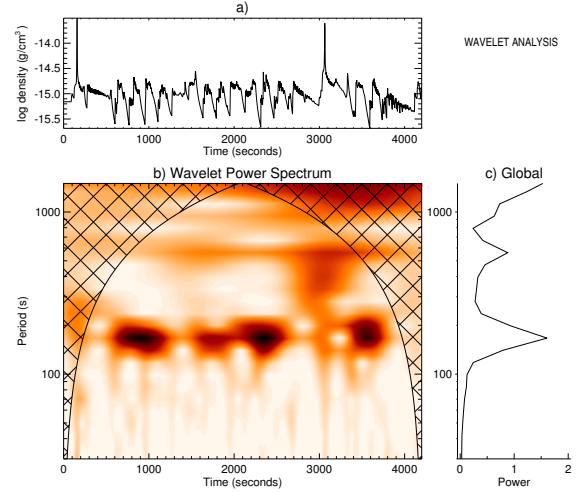


Fig. 5. (a) Variation of the summit density with time for a loop length $L = 10$ Mm and pulses injected over segments of length $0.1 L$ from the loop's footpoints. (b) Wavelet power analysis of the summit density in (a).

period though negative (e.g. between $t=1400-2000$ s). However this apparent contradiction can be resolved because the direction of velocity is defined arbitrarily. By introducing a new coordinate system with opposite positive direction along the loop, the phase shift will be positive again. We conclude, that, so far the calculated density and velocity oscillations could be intermittent standing waves set up by random energy releases.

Next, we study the wavelet of the density time series. The wavelet power spectrum (WPS; Torrence & Compo 1998) of the apex density time series is shown in the bottom panel of Figure 5. The wavelet confidence level is of 95%. The power spectrum indicates several interesting features. The WPS clearly shows various coherent global periodicities in the evolution of density as a result of the response of the medium to an impulsive energy release.

A clear band of wavelet power above the confidence level, within the cone of influence (COI), and, centered around a period of 550 s is found. This somewhat long period can be driven by internal gravity waves. The period of such waves can be estimated by the inverse of the cutoff frequency $\Omega = (\gamma g_{\odot} / 2C_s)$. Estimates for the considered simulated loop give values of the order of 520 s which matches well with the value obtained from the wavelet analysis.

Figure 5 also shows that a series of beads or periodic patterns at around 900 s, 1800 s, 2400 s and 3600 s of the evolution appear with a dominant period of order of $P = 150 - 220$ s. These patterns are bounded within a time interval of approximately 600 s in-

dicating the appearance of wave packets similar to those produced by interference. Recently, McIntosh & Smillie (2004) used wavelet transforms to study the characteristic time scales of chromospheric oscillation wave packets that are observed in Transition Region and Coronal Explorer (TRACE) ultraviolet continuum image time series. Using several data sets, they investigated the statistical, spatial and temporal intermittence of the number, duration, mean frequency, and delay (wait time) between wave packets in the time series data. In our simulations, we observe these types of wave packets and the same terminology could be used. The periods involved for the generation of these interference patterns cannot be resolved with wavelet analysis, instead we have used the Lomb-Scargle periodogram, a modified version developed by Carbonell & Ballester (1991) to compute these periods. These close periods are obtained and are of the order of 183 and 223 s (~ 5 mHz).

We also investigated how the effect of changing the length of the loop segment, ΔL , where the random energy releases occur.

Increasing the size ΔL of the loop segment along which the pulses are randomly distributed but keeping fixed the other parameters we observe a similar oscillatory pattern as in Figure 4. This time the maximum of the dominant period is slightly decreased to ≈ 145 s. Computing a long time series evolution (up to 12000 s) one finds that the packets are more frequent than for smaller ΔL . If ΔL is further increased, say to $0.5 L$, i.e. the pulses were distributed randomly along the whole loop (though these pulses are still randomly distributed in space and time), the oscillatory patterns are even more frequent in the entire evolution. It was seen that the dominant periods are even smaller than in the previous cases of shorter segment of random energy distribution. At this stage one can conclude, that distributing the pulses more widely in the whole loop produce oscillations at a certain period that is around 120 seconds.

We recall the simple estimate equation derived by Roberts et al. (1984) that relates for standing waves the period, loop length, and, wave speed for the fundamental mode

$$P = \frac{2L}{C_s} = \frac{2L}{1.18 \times 10^4 \sqrt{T}}, \quad (2)$$

where C_s is the speed of sound and T measured in MK while L is in centimeters. If we substitute the loop length $L = 10$ Mm and the average temperature of 1 MK for the whole evolution for the simulated

case with $\Delta L/L = 0.1$ we obtained a period of the order of 170 s. Díaz (2005, private comm.) derived a simple wave equation for the slow modes of coronal structures using stretching coordinates (Roberts 2005) to decouple them from the rest of the MHD modes. He obtained the corrected periods with respect to the results of the homogeneous tube calculated with equation (2) of the order of 175.3 s. With these results, one can see that improving the model by including more detailed physics improves the estimated period.

We would like to thank the CDCHT of the Universidad de los Andes for financial support (C-1271-04-05-A).

REFERENCES

- Asai, A., et al. 2001, *ApJ*, 562, L103
 Aschwanden, M. J., Fletcher, L., Schrijver, C. J., & Alexander, D. 1999, *ApJ*, 520, 880
 Aschwanden, M. J. 2004, *Coronal Heating*, ed. R. W. Walsh, J. Ireland, D. Danesy, & B. Fleck (ESA SP-575; Noordwijk: ESA), 97
 Braginskii, S. I. 1965, *Rev. Plasma Phys.*, 1, 205
 Carbonell, M., & Ballester, J. L. 1991, *A&A*, 249, 295
 Hildner, E. 1974, *Sol. Phys.*, 35, 23
 Kjeldseth-Moe, O., & Brekke, P. 1998, *Sol. Phys.*, 182, 73
 Kliem, B., Dammasch, I. E., Curdt, W., & Wilhelm, K. 2002, *ApJ*, 568, L61
 McIntosh, S. W., & Smillie, D. G. 2004, *ApJ*, 604, 924
 Mendoza-Briceño, C. A., Sigalotti, L. Di G., & Erdélyi, R. 2005, *ApJ*, 624, 1080
 Nakariakov, V. M., Ofman, L., DeLuca, E. E., Roberts, B., & Davila, J. M. 1999, *Science*, 285, 862
 Nakariakov, V. M., & Ofman, L. 2001, *A&A*, 372, L53
 Ofman, L., & Wang, T. 2002, *ApJ*, 580, L85
 Roberts, B. 2005, *Philos. Trans. Royal Soc. London A*, 2006, 364, 447
 Roberts, B., Edwin, P. M., & Benz, A. O. 1984, *ApJ*, 279, 857
 Sakurai, T., Ichimoto, K., Raju, K. P., & Singh, J. 2002, *Sol. Phys.*, 209, 265
 Schrijver, C. J. 2001, *Sol. Phys.*, 198, 325
 Torrence, C., & Compo, G. P. 1998, *Bull. Am. Meteorol. Soc.*, 79, 61
 Wang, T. J., Solanki, S. K., Curdt, W., Innes, D. E., & Dammasch, I. E. 2002a, *From Solar Minimum to Maximum*, ed. A. Wilson (ESA SP-508; Noordwijk: ESA), 465
 ———. 2002b, *ApJ*, 574, L101
 Wang, T. J., Solanki, S. K., Curdt, W., Innes, D. E., Dammasch, I. E., & Kliem, B. 2003a, *A&A*, 406, 1105
 Wang, T. J., Solanki, S. K., Innes, D. E., Curdt, W., & Marsch, E. 2003b, *A&A*, 402, L17
 Wang, T. J., Solanki, S. K., Innes, D. E., & Curdt, W. 2005, *A&A*, 435, 753